



Measurement of b -hadron masses[☆]

LHCb Collaboration

ARTICLE INFO

Article history:

Received 21 December 2011

Received in revised form 19 January 2012

Accepted 20 January 2012

Available online 24 January 2012

Editor: W.-D. Schlatter

ABSTRACT

Measurements of b -hadron masses are performed with the exclusive decay modes $B^+ \rightarrow J/\psi K^+$, $B^0 \rightarrow J/\psi K^{*0}$, $B^0 \rightarrow J/\psi K_S^0$, $B_s^0 \rightarrow J/\psi \phi$ and $\Lambda_b^0 \rightarrow J/\psi \Lambda$ using an integrated luminosity of 35 pb^{-1} collected in pp collisions at a centre-of-mass energy of 7 TeV by the LHCb experiment. The momentum scale is calibrated with $J/\psi \rightarrow \mu^+ \mu^-$ decays and verified to be known to a relative precision of 2×10^{-4} using other two-body decays. The results are more precise than previous measurements, particularly in the case of the B_s^0 and Λ_b^0 masses.

© 2012 CERN. Published by Elsevier B.V. Open access under CC BY-NC-ND license.

1. Introduction

Within the Standard Model of particle physics, mesons and baryons are colourless objects composed of quarks and gluons. These systems are bound through the strong interaction, described by quantum chromodynamics (QCD). A basic property of hadrons that can be compared to theoretical predictions is their masses. The most recent theoretical predictions based on lattice QCD calculations can be found in Refs. [1,2]. The current experimental knowledge of the b -hadron masses as summarized in Ref. [3] is dominated by results from the CDF Collaboration [4]. In this Letter precision measurements of the masses of the B^+ , B^0 , B_s^0 and Λ_b^0 are presented as well as the mass splittings with respect to the B^+ . The results are based on a data sample of proton–proton collisions at $\sqrt{s} = 7 \text{ TeV}$ at the Large Hadron Collider collected by the LHCb experiment, corresponding to an integrated luminosity of 35 pb^{-1} .

The LHCb detector [5] is a forward spectrometer providing charged particle reconstruction in the pseudorapidity range $2 < \eta < 5$. The most important elements for the analysis presented here are precision tracking and excellent particle identification. The tracking system consists of a silicon strip vertex detector (VELO) surrounding the pp interaction region, a large area silicon strip detector located upstream of a dipole magnet with a bending power of about 4 Tm, and a combination of silicon strip detectors and straw drift-tubes placed downstream. The combined tracking system has a momentum resolution $\delta p/p$ that varies from 0.4% at 5 GeV/c to 0.6% at 100 GeV/c. Pion, kaon and proton separation is provided by two ring imaging Cherenkov (RICH) detectors whilst muons are identified by a muon system consisting of alternating layers of iron and multi-wire proportional chambers.

The data used for this analysis were collected in 2010. The trigger system consists of two levels. The first stage is implemented in hardware and uses information from the calorimeters and the muon system. The second stage is implemented in software and runs on an event filter farm. Dedicated trigger lines collect events containing J/ψ mesons. For this analysis all events are used regardless of which trigger line fired.

Simulation samples used are based on the PYTHIA 6.4 generator [6] configured with the parameters detailed in Ref. [7]. QED final state radiative corrections are included using the PHOTOS package [8]. The EVTGEN [9] and GEANT4 [10] packages are used to generate hadron decays and simulate interactions in the detector, respectively.

The alignment of the tracking system, as well as the calibration of the momentum scale based on the $J/\psi \rightarrow \mu^+ \mu^-$ mass peak, were carried out in seven time periods corresponding to different running conditions. The procedure takes into account the effects of QED radiative corrections which are important in the $J/\psi \rightarrow \mu^+ \mu^-$ decay. Fig. 1 shows that the reconstructed J/ψ mass after alignment and calibration is stable in time to better than 0.02% throughout the data-taking period. The validity of the momentum calibration has been checked using samples of $K_S^0 \rightarrow \pi^+ \pi^-$, $D^0 \rightarrow K^- \pi^+$, $\bar{D}^0 \rightarrow K^+ \pi^-$, $\psi(2S) \rightarrow \mu^+ \mu^-$, $\Upsilon(1S) \rightarrow \mu^+ \mu^-$ and $\Upsilon(2S) \rightarrow \mu^+ \mu^-$ decays. In each case the mass distribution is modelled taking into account the effect of radiative corrections, resolution and background, and the mean mass value extracted. To allow comparison between the decay modes, the deviation of the measured mass from the expected value [3] is converted into an estimate of the momentum scale bias, referred to as α . This is defined such that the measured mass is equal to the expected value if all particle momenta are multiplied by $1 - \alpha$. Fig. 2 shows the resulting values of α . The deviation for the considered modes is $\pm 0.02\%$, which is taken as the systematic uncertainty on the momentum scale.

[☆] © CERN for the benefit of the LHCb Collaboration.

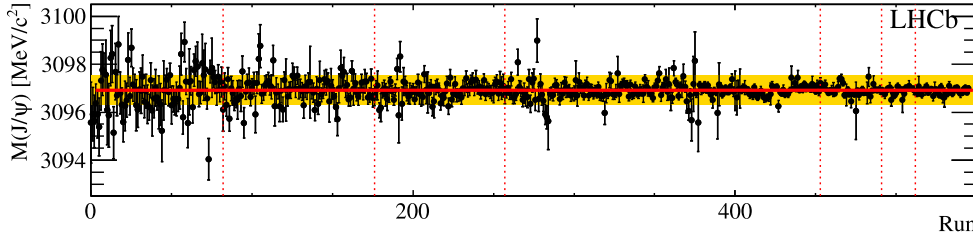


Fig. 1. Reconstructed $J/\psi \rightarrow \mu^+\mu^-$ fitted mass as a function of run number after the momentum calibration procedure discussed in the text. The vertical dashed lines indicate the boundaries of the seven calibration periods. A fit of a constant function (horizontal line) has a χ^2 probability of 6%. The shaded area corresponds to the assigned uncertainty on the momentum scale of 0.02%.

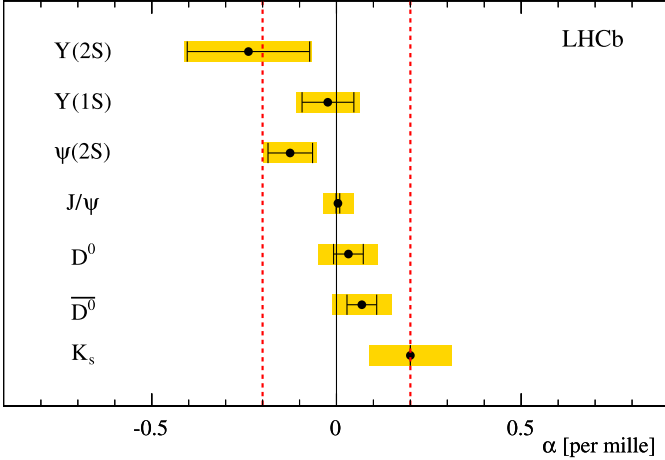


Fig. 2. Momentum scale bias α , extracted from the reconstructed mass of various two-body decays after the momentum calibration procedure described in the text. By construction one expects $\alpha = 0$ for the $J/\psi \rightarrow \mu^+\mu^-$ calibration mode. The black error bars represent the statistical uncertainty whilst the (yellow) shaded areas include contributions to the systematic error from the fitting procedure, the effect of QED radiative corrections and the uncertainty quoted by the PDG [3] on the mass of the decaying meson. The (red) dashed lines correspond to the assigned uncertainty on the momentum scale of 0.02%. (For interpretation of the references to colour in this figure legend, the reader is referred to the web version of this Letter.)

2. Event selection

A common strategy, aiming at high signal purity, is adopted for the reconstruction and selection of $B^+ \rightarrow J/\psi K^+$, $B^0 \rightarrow J/\psi K^{*0}$, $B^0 \rightarrow J/\psi K_S^0$, $B_s^0 \rightarrow J/\psi \phi$ and $\Lambda_b^0 \rightarrow J/\psi \Lambda$ candidates (the inclusion of charge-conjugated modes is implied throughout). In general, only tracks traversing the whole spectrometer are used; however, since K_S^0 and Λ particles may decay outside of the VELO, pairs of tracks without VELO hits are also used to build K_S^0 and Λ candidates. The χ^2 per number of degrees of freedom (χ^2/ndf) of the track fit is required to be smaller than four. The Kullback–Leibler (KL) distance [11] is used to identify pairs of reconstructed tracks that are very likely to arise from hits created by the same charged particle: if two reconstructed tracks have a symmetrized KL divergence less than 5000, only that with the higher fit quality is considered.

$J/\psi \rightarrow \mu^+\mu^-$ candidates are formed from pairs of oppositely-charged muons with a transverse momentum (p_T) larger than 0.5 GeV/c, originating from a common vertex with $\chi^2/\text{ndf} < 11$, and satisfying $|M_{\mu\mu} - M_{J/\psi}| < 3\sigma$ where $M_{\mu\mu}$ is the reconstructed dimuon mass, $M_{J/\psi}$ is the known J/ψ mass world average value [3], and σ is the estimated event-by-event uncertainty on $M_{\mu\mu}$. The selected J/ψ candidates are then combined with one of K^+ , $K^{*0} \rightarrow K^+\pi^-$, $\phi \rightarrow K^+K^-$, $K_S^0 \rightarrow \pi^+\pi^-$ or $\Lambda \rightarrow p\pi^-$ to create b -hadron candidates. Mass windows

of $\pm 70 \text{ MeV}/c^2$, $\pm 12 \text{ MeV}/c^2$, $\pm 12 \text{ MeV}/c^2$ ($\pm 21 \text{ MeV}/c^2$) and $\pm 6 \text{ MeV}/c^2$ ($\pm 6 \text{ MeV}/c^2$) around the world averages [3] are used to select the K^{*0} , ϕ , K_S^0 and Λ candidates formed from tracks with (without) VELO hits, respectively. Kaons are selected by cutting on the difference between the log-likelihoods of the kaon and pion hypotheses provided by the RICH detectors ($\Delta \ln \mathcal{L}_{K-\pi} > 0$). To eliminate background from $B_s^0 \rightarrow J/\psi \phi$ in the $B^0 \rightarrow J/\psi K^{*0}$ channel, the pion from the K^{*0} candidate is required to be inconsistent with the kaon hypothesis ($\Delta \ln \mathcal{L}_{K-\pi} < 0$). To further improve the signal purity, a requirement of $p_T > 1 \text{ GeV}/c$ is applied on the particle associated with the J/ψ candidate. For final states including a V^0 (K_S^0 or Λ), an additional requirement of $L/\sigma_L > 5$ is made, where L is the distance between the b -hadron and the V^0 decay vertex, and σ_L is the uncertainty on this quantity.

Each b -hadron candidate is associated with the reconstructed pp primary interaction vertex with respect to which it has the smallest impact parameter significance, and this significance is required to be less than five. As there is a large combinatorial background due to particles originating directly from the pp primary vertex, only b -hadron candidates with a reconstructed decay time greater than 0.3 ps are considered for subsequent analysis. A decay chain fit [12] is performed for each candidate, which constrains the reconstructed J/ψ mass and, if applicable, the reconstructed K_S^0 or Λ mass to their nominal values [3]. The χ^2/ndf of the fit is required to be smaller than five. The mass of the b -hadron candidate is obtained from this fit and its estimated uncertainty is required to be smaller than $20 \text{ MeV}/c^2$.

3. Results

The b -hadron masses are determined by performing unbinned maximum likelihood fits to the invariant mass distributions, in which the signal and background components are described by a Gaussian and an exponential function, respectively. Alternative models for both the signal and background components are considered as part of the systematic studies. Fig. 3 shows the invariant mass distributions and fits for the five modes considered in this study. The signal yields, mass values and resolutions resulting from the fits are given in Table 1.

The presence of biases due to neglecting QED radiative corrections in the mass fits is studied using a simulation based on PHOTOS [8]. The fitted masses quoted in Table 1 for the $B^+ \rightarrow J/\psi K^+$ and $B^0 \rightarrow J/\psi K^{*0}$ are found to be underestimated by $0.14 \pm 0.01 \text{ MeV}/c^2$ and $0.11 \pm 0.01 \text{ MeV}/c^2$, respectively, when radiative corrections are ignored; they are therefore corrected for these biases, and the uncertainty is propagated as a systematic effect. The bias for the $B_s^0 \rightarrow J/\psi \phi$ mode is negligible due to the restricted phase space for the kaons from the ϕ decay. There is no bias for the $B^0 \rightarrow J/\psi K_S^0$ and $\Lambda_b^0 \rightarrow J/\psi \Lambda$ modes since the J/ψ , K_S^0 and Λ masses are constrained in the vertex fits.

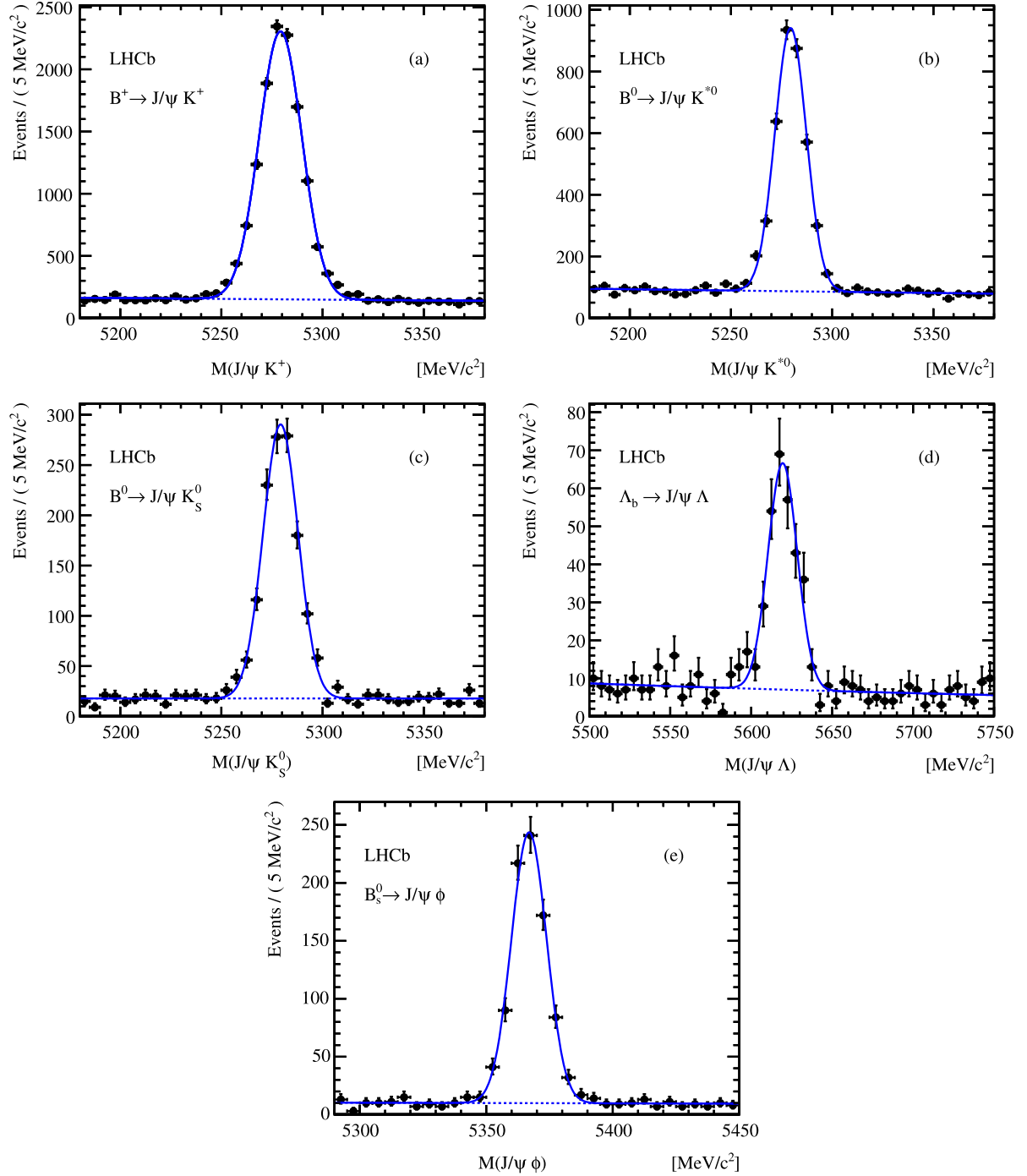


Fig. 3. Invariant mass distributions for (a) $B^+ \rightarrow J/\psi K^+$, (b) $B^0 \rightarrow J/\psi K^{*0}$, (c) $B^0 \rightarrow J/\psi K_S^0$, (d) $\Lambda_b^0 \rightarrow J/\psi \Lambda$, and (e) $B_s^0 \rightarrow J/\psi \phi$ candidates. In each case the result of the fit described in the text is superimposed (solid line) together with the background component (dotted line).

Table 1

Signal yields, mass values and mass resolutions obtained from the fits shown in Fig. 3 together with the values corrected for the effect of QED radiative corrections as described in the text. The quoted uncertainties are statistical.

Decay mode	Yield	Fitted mass [MeV/c ²]	Corrected mass [MeV/c ²]	Resolution [MeV/c ²]
$B^+ \rightarrow J/\psi K^+$	$11\,151 \pm 115$	5279.24 ± 0.11	5279.38 ± 0.11	10.5 ± 0.1
$B^0 \rightarrow J/\psi K^{*0}$	3308 ± 65	5279.47 ± 0.17	5279.58 ± 0.17	7.7 ± 0.2
$B^0 \rightarrow J/\psi K_S^0$	1184 ± 38	5279.58 ± 0.29	5279.58 ± 0.29	8.6 ± 0.3
$B_s^0 \rightarrow J/\psi \phi$	816 ± 30	5366.90 ± 0.28	5366.90 ± 0.28	7.0 ± 0.3
$\Lambda_b^0 \rightarrow J/\psi \Lambda$	279 ± 19	5619.19 ± 0.70	5619.19 ± 0.70	9.0 ± 0.6

Table 2Systematic uncertainties (in MeV/c^2) on the mass measurements.

Source of uncertainty	$B^+ \rightarrow J/\psi K^+$	$B^0 \rightarrow J/\psi K^{*0}$	$B^0 \rightarrow J/\psi K_S^0$	$B_s^0 \rightarrow J/\psi \phi$	$\Lambda_b^0 \rightarrow J/\psi \Lambda$
Mass fitting:					
– Background model	0.04	0.03	<0.01	0.01	<0.01
– Resolution model	0.01	0.02	0.06	0.02	0.07
– Radiative corrections	0.01	0.01	–	–	–
Momentum calibration:					
– Average momentum scale	0.30	0.27	0.30	0.22	0.27
– η dependence of momentum scale	0.04	<0.01	0.09	0.03	0.02
Detector description:					
– Energy loss correction	0.10	<0.01	0.05	0.03	0.09
Detector alignment:					
– Vertex detector (track slopes)	0.05	0.04	0.04	0.03	0.04
Quadratic sum	0.33	0.27	0.33	0.23	0.30

Table 3Systematic uncertainties (in MeV/c^2) on the differences of mass measurements, expressed with respect to the $B^+ \rightarrow J/\psi K^+$ mass (e.g. the last column gives the systematic uncertainties on $M(\Lambda_b^0 \rightarrow J/\psi \Lambda) - M(B^+ \rightarrow J/\psi K^+)$).

Source of uncertainty	$B^0 \rightarrow J/\psi K^{*0}$	$B^0 \rightarrow J/\psi K_S^0$	$B_s^0 \rightarrow J/\psi \phi$	$\Lambda_b^0 \rightarrow J/\psi \Lambda$
Mass fitting:				
– Background model	0.05	0.04	0.04	0.04
– Resolution model	0.02	0.06	0.02	0.07
– Radiative corrections	<0.01	0.01	0.01	0.01
Momentum calibration:				
– Average momentum scale	0.03	<0.01	0.08	0.03
– η dependence of momentum scale	0.04	0.05	0.01	0.02
Detector description:				
– Energy loss correction	0.10	0.05	0.07	0.01
Detector alignment:				
– Vertex detector (track slopes)	0.01	0.01	0.02	0.01
Quadratic sum	0.12	0.10	0.12	0.09

4. Systematic studies and checks

To evaluate the systematic error, the complete analysis is repeated (including the track fit and the momentum scale calibration when needed), varying within their uncertainties the parameters to which the mass determination is sensitive. The observed changes in the central values of the fitted masses relative to the nominal results are then assigned as systematic uncertainties.

The dominant source of uncertainty is the limited knowledge of the momentum scale. The mass fits are repeated with the momentum scale varied by $\pm 0.02\%$. After the calibration procedure a $\pm 0.07\%$ variation of the momentum scale remains as a function of the particle pseudorapidity η . To first order the effect of this averages out in the mass determination. The residual impact of this variation is evaluated by parameterizing the momentum scale as a function of η and repeating the analysis. The amount of material traversed in the tracking system by a particle is known to 10% accuracy [13]; the magnitude of the energy loss correction in the reconstruction is therefore varied by 10%. To ensure the detector alignment is well understood a further test is carried out: the horizontal and vertical slopes of the tracks close to the interaction region, which are determined by measurements in the VELO, are changed by 1×10^{-3} , corresponding to the precision with which the length scale along the beam axis is known [14]. Other uncertainties arise from the fit modelling: a double Gaussian function (with common mean) for the signal resolution and/or a flat background component are used instead of the nominal Gaussian and exponential functions. The effect of possible reflections due to particle mis-identification is small and can be neglected. Finally, a systematic uncertainty related to the evaluation of the effect of the radiative corrections is assigned. Tables 2 and 3 summarize the systematic uncertainties assigned on the measured masses and mass differences.

The stability of the measured b -hadron masses is studied by dividing the data samples according to the polarity of the spectrometer magnet, final state flavour (for modes where the final state is flavour specific), as well as whether the K_S^0 and Λ daughter particles have VELO hits. As a cross-check the analysis is repeated ignoring the hits from the tracking station before the magnet. This leads to an average shift in measured masses compatible with statistical fluctuations. In addition, for the B^+ and B^0 modes where the event samples are sizable, the measurements are repeated in bins of the b -hadron kinematic variables. None of these checks reveals a systematic bias.

5. Conclusions

The b -hadron masses are measured using data collected in 2010 at a centre-of-mass energy of $\sqrt{s} = 7$ TeV. The results are

$$\begin{aligned}
 M(B^+ J/\psi K^+) &= 5279.38 \pm 0.11 \text{ (stat)} \pm 0.33 \text{ (syst)} \text{ MeV}/c^2, \\
 M(B^0 J/\psi K^{*0}) &= 5279.58 \pm 0.15 \text{ (stat)} \pm 0.28 \text{ (syst)} \text{ MeV}/c^2, \\
 M(B_s^0 J/\psi \phi) &= 5366.90 \pm 0.28 \text{ (stat)} \pm 0.23 \text{ (syst)} \text{ MeV}/c^2, \\
 M(\Lambda_b^0 J/\psi \Lambda) &= 5619.19 \pm 0.70 \text{ (stat)} \pm 0.30 \text{ (syst)} \text{ MeV}/c^2,
 \end{aligned}$$

where the B^0 result is obtained as a weighted average of $M(B^0 \rightarrow J/\psi K^{*0}) = 5279.58 \pm 0.17 \pm 0.27 \text{ MeV}/c^2$ and $M(B^0 \rightarrow J/\psi K_S^0) = 5279.58 \pm 0.29 \pm 0.33 \text{ MeV}/c^2$ assuming all systematic uncertainties to be correlated, except those related to the mass model. The dominant systematic uncertainty is related to the knowledge of the average momentum scale of the tracking system. It largely cancels in the mass differences. We obtain

$$\begin{aligned}
 M(B^0 \rightarrow J/\psi K^{*0}) - M(B^+ \rightarrow J/\psi K^+) \\
 = 0.20 \pm 0.17 \text{ (stat)} \pm 0.11 \text{ (syst)} \text{ MeV}/c^2,
 \end{aligned}$$

Table 4

LHCb measurements, compared to both the best previous measurements and the results of a global fit to available b -hadron mass data [3]. The quoted errors include statistical and systematic uncertainties. All values are in MeV/c^2 .

Quantity	LHCb measurement	Best previous measurement	PDG fit
$M(B^+)$	5279.38 ± 0.35	5279.10 ± 0.55 [4]	5279.17 ± 0.29
$M(B^0)$	5279.58 ± 0.32	5279.63 ± 0.62 [4]	5279.50 ± 0.30
$M(B_s^0)$	5366.90 ± 0.36	5366.01 ± 0.80 [4]	5366.3 ± 0.6
$M(\Lambda_b^0)$	5619.19 ± 0.76	5619.7 ± 1.7 [4]	–
$M(B^0) - M(B^+)$	0.20 ± 0.20	0.33 ± 0.06 [15]	0.33 ± 0.06
$M(B_s^0) - M(B^+)$	87.52 ± 0.32	–	–
$M(\Lambda_b^0) - M(B^+)$	339.81 ± 0.72	–	–

$$M(B_s^0 \rightarrow J/\psi\phi) - M(B^+ \rightarrow J/\psi K^+) \\ = 87.52 \pm 0.30 \text{ (stat)} \pm 0.12 \text{ (syst)} \text{ MeV}/c^2,$$

$$M(\Lambda_b^0 \rightarrow J/\psi\Lambda) - M(B^+ \rightarrow J/\psi K^+) \\ = 339.81 \pm 0.71 \text{ (stat)} \pm 0.09 \text{ (syst)} \text{ MeV}/c^2,$$

where the B^0 result is a combination of $M(B^0 \rightarrow J/\psi K^{*0}) - M(B^+ \rightarrow J/\psi K^+) = 0.20 \pm 0.20 \pm 0.12 \text{ MeV}/c^2$ and $M(B^0 \rightarrow J/\psi K_S^0) - M(B^+ \rightarrow J/\psi K^+) = 0.20 \pm 0.31 \pm 0.10 \text{ MeV}/c^2$ under the same hypothesis as above.

As shown in Table 4, our measurements are in agreement with previous measurements [3,4]. Besides the difference between the B^+ and B^0 masses they are the most accurate to date, with significantly improved precision over previous measurements in the case of the B_s^0 and Λ_b^0 masses.

Acknowledgements

We would like to thank our colleague Adlène Hicheur who made, as a member of our collaboration, significant contributions to the tracking alignment algorithms and provided the first realistic version of the magnetic field map. He is currently unable to continue his work, and we hope that this situation will be resolved soon. We express our gratitude to our colleagues in the CERN accelerator departments for the excellent performance of the LHC.

LHCb Collaboration

R. Aaij²³, C. Abellan Beteta^{35,n}, B. Adeva³⁶, M. Adinolfi⁴², C. Adrover⁶, A. Affolder⁴⁸, Z. Ajaltouni⁵, J. Albrecht³⁷, F. Alessio³⁷, M. Alexander⁴⁷, G. Alkhazov²⁹, P. Alvarez Cartelle³⁶, A.A. Alves Jr.²², S. Amato², Y. Amhis³⁸, J. Anderson³⁹, R.B. Appleby⁵⁰, O. Aquines Gutierrez¹⁰, F. Archilli^{18,37}, L. Arrabito⁵³, A. Artamonov³⁴, M. Artuso^{52,37}, E. Aslanides⁶, G. Auriemma^{22,m}, S. Bachmann¹¹, J.J. Back⁴⁴, D.S. Bailey⁵⁰, V. Balagura^{30,37}, W. Baldini¹⁶, R.J. Barlow⁵⁰, C. Barschel³⁷, S. Barsuk⁷, W. Barter⁴³, A. Bates⁴⁷, C. Bauer¹⁰, Th. Bauer²³, A. Bay³⁸, I. Bediaga¹, S. Belogurov³⁰, K. Belous³⁴, I. Belyaev^{30,37}, E. Ben-Haim⁸, M. Benayoun⁸, G. Bencivenni¹⁸, S. Benson⁴⁶, J. Benton⁴², R. Bernet³⁹, M.-O. Bettler¹⁷, M. van Beuzekom²³, A. Bien¹¹, S. Bifani¹², T. Bird⁵⁰, A. Bizzeti^{17,h}, P.M. Bjørnstad⁵⁰, T. Blake³⁷, F. Blanc³⁸, C. Blanks⁴⁹, J. Blouw¹¹, S. Blusk⁵², A. Bobrov³³, V. Bocci²², A. Bondar³³, N. Bondar²⁹, W. Bonivento¹⁵, S. Borghi^{47,50}, A. Borgia⁵², T.J.V. Bowcock⁴⁸, C. Bozzi¹⁶, T. Brambach⁹, J. van den Brand²⁴, J. Bressieux³⁸, D. Brett⁵⁰, M. Britsch¹⁰, T. Britton⁵², N.H. Brook⁴², A. Büchler-Germann³⁹, I. Burducea²⁸, A. Bursche³⁹, J. Buytaert³⁷, S. Cadeddu¹⁵, O. Callot⁷, M. Calvi^{20,j}, M. Calvo Gomez^{35,n}, A. Camboni³⁵, P. Campana^{18,37}, A. Carbone¹⁴, G. Carboni^{21,k}, R. Cardinale^{19,37,i}, A. Cardini¹⁵, L. Carson⁴⁹, K. Carvalho Akiba², G. Casse⁴⁸, M. Cattaneo³⁷, Ch. Cauet⁹, M. Charles⁵¹, Ph. Charpentier³⁷, N. Chiapolini³⁹, K. Ciba³⁷, X. Cid Vidal³⁶, G. Ciezarek⁴⁹, P.E.L. Clarke^{46,37}, M. Clemencic³⁷, H.V. Cliff⁴³, J. Closier³⁷, C. Coca²⁸, V. Coco²³, J. Cogan⁶, P. Collins³⁷,

We thank the technical and administrative staff at CERN and at the LHCb institutes, and acknowledge support from the National Agencies: CAPES, CNPq, FAPERJ and FINEP (Brazil); CERN; NSFC (China); CNRS/IN2P3 (France); BMBF, DFG, HGF and MPG (Germany); SFI (Ireland); INFN (Italy); FOM and NWO (The Netherlands); SCSR (Poland); ANCS (Romania); MinES of Russia and Rosatom (Russia); MICINN, XuntaGal and GENCAT (Spain); SNSF and SER (Switzerland); NAS Ukraine (Ukraine); STFC (United Kingdom); NSF (USA). We also acknowledge the support received from the ERC under FP7 and the Region Auvergne.

Open access

This article is published Open Access at sciencedirect.com. It is distributed under the terms of the Creative Commons Attribution License 3.0, which permits unrestricted use, distribution, and reproduction in any medium, provided the original authors and source are credited.

References

- [1] E.B. Gregory, et al., Phys. Rev. D 83 (2011) 014506, arXiv:1010.3848.
- [2] R. Lewis, R.M. Woloshyn, Phys. Rev. D 79 (2009) 014502, arXiv:0806.4783.
- [3] Particle Data Group, K. Nakamura, et al., J. Phys. G 37 (2010) 075021.
- [4] CDF Collaboration, D. Acosta, et al., Phys. Rev. Lett. 96 (2006) 202001, arXiv:hep-ex/0508022.
- [5] LHCb Collaboration, A.A. Alves Jr., et al., JINST 3 (2008) S08005.
- [6] T. Sjöstrand, S. Mrenna, P.Z. Skands, JHEP 0605 (2006) 026, arXiv:hep-ph/0603175.
- [7] I. Belyaev, et al., IEEE (2010) 1155.
- [8] E. Barberio, Z. Wąs, Comput. Phys. Commun. 79 (1994) 291.
- [9] D.J. Lange, Nucl. Instrum. Meth. A 462 (2001) 152.
- [10] GEANT4 Collaboration, S. Agostinelli, et al., Nucl. Instrum. Meth. A 506 (2003) 250.
- [11] S. Kullback, R.A. Leibler, Ann. Math. Statist. 22 (1951) 79; S. Kullback, Amer. Statist. 41 (1987) 340; The use of the Kullback–Leibler distance is described in M. Needham, Clone track identification using the Kullback–Leibler distance, LHCb-2008-002.
- [12] W.D. Hulsbergen, Nucl. Instrum. Meth. A 552 (2005) 566, arXiv:physics/0503191.
- [13] LHCb Collaboration, R. Aaij, et al., Phys. Lett. 693 (2010) 69, arXiv:1008.3105.
- [14] LHCb Collaboration, R. Aaij, et al., Phys. Lett. B (2011), submitted for publication, arXiv:1112.4311.
- [15] BaBar Collaboration, B. Aubert, et al., Phys. Rev. D 78 (2008) 011103, arXiv:0805.0497.

A. Comerma-Montells³⁵, F. Constantin²⁸, A. Contu⁵¹, A. Cook⁴², M. Coombes⁴², G. Corti³⁷, G.A. Cowan³⁸, R. Currie⁴⁶, C. D'Ambrosio³⁷, P. David⁸, P.N.Y. David²³, I. De Bonis⁴, S. De Capua^{21,k}, M. De Cian³⁹, F. De Lorenzi¹², J.M. De Miranda¹, L. De Paula², P. De Simone¹⁸, D. Decamp⁴, M. Deckenhoff⁹, H. Degaudenzi^{38,37}, L. Del Buono⁸, C. Deplano¹⁵, D. Derkach^{14,37}, O. Deschamps⁵, F. Dettori²⁴, J. Dickens⁴³, H. Dijkstra³⁷, P. Diniz Batista¹, F. Domingo Bonal^{35,n}, S. Donleavy⁴⁸, F. Dordei¹¹, A. Dosil Suárez³⁶, D. Dossett⁴⁴, A. Dovbnya⁴⁰, F. Dupertuis³⁸, R. Dzhelyadin³⁴, A. Dziurda²⁵, S. Easo⁴⁵, U. Egede⁴⁹, V. Egorychev³⁰, S. Eidelman³³, D. van Eijk²³, F. Eisele¹¹, S. Eisenhardt⁴⁶, R. Ekelhof⁹, L. Eklund⁴⁷, Ch. Elsasser³⁹, D. Elsby⁵⁵, D. Esperante Pereira³⁶, L. Estève⁴³, A. Falabella^{16,14,e}, E. Fanchini^{20,j}, C. Färber¹¹, G. Fardell⁴⁶, C. Farinelli²³, S. Farry¹², V. Fave³⁸, V. Fernandez Albor³⁶, M. Ferro-Luzzi³⁷, S. Filippov³², C. Fitzpatrick⁴⁶, M. Fontana¹⁰, F. Fontanelli^{19,i}, R. Forty³⁷, M. Frank³⁷, C. Frei³⁷, M. Frosini^{17,37,f}, S. Furcas²⁰, A. Gallas Torreira³⁶, D. Galli^{14,c}, M. Gandelman², P. Gandini⁵¹, Y. Gao³, J.-C. Garnier³⁷, J. Garofoli⁵², J. Garra Tico⁴³, L. Garrido³⁵, D. Gascon³⁵, C. Gaspar³⁷, N. Gauvin³⁸, M. Gersabeck³⁷, T. Gershon^{44,37}, Ph. Ghez⁴, V. Gibson⁴³, V.V. Gligorov³⁷, C. Göbel⁵⁴, D. Golubkov³⁰, A. Golutvin^{49,30,37}, A. Gomes², H. Gordon⁵¹, M. Grabalosa Gándara³⁵, R. Graciani Diaz³⁵, L.A. Granado Cardoso³⁷, E. Graugés³⁵, G. Graziani¹⁷, A. Grecu²⁸, E. Greening⁵¹, S. Gregson⁴³, B. Gui⁵², E. Gushchin³², Yu. Guz³⁴, T. Gys³⁷, G. Haefeli³⁸, C. Haen³⁷, S.C. Haines⁴³, T. Hampson⁴², S. Hansmann-Menzemer¹¹, R. Harji⁴⁹, N. Harnew⁵¹, J. Harrison⁵⁰, P.F. Harrison⁴⁴, T. Hartmann⁵⁶, J. He⁷, V. Heijne²³, K. Hennessy⁴⁸, P. Henrard⁵, J.A. Hernando Morata³⁶, E. van Herwijnen³⁷, E. Hicks⁴⁸, K. Holubyev¹¹, P. Hopchev⁴, W. Hulsbergen²³, P. Hunt⁵¹, T. Huse⁴⁸, R.S. Huston¹², D. Hutchcroft⁴⁸, D. Hynds⁴⁷, V. Iakovenko⁴¹, P. Ilten¹², J. Imong⁴², R. Jacobsson³⁷, A. Jaeger¹¹, M. Jahjah Hussein⁵, E. Jans²³, F. Jansen²³, P. Jatun³⁸, B. Jean-Marie⁷, F. Jing³, M. John⁵¹, D. Johnson⁵¹, C.R. Jones⁴³, B. Jost³⁷, M. Kabbalo⁹, S. Kandybei⁴⁰, M. Karacson³⁷, T.M. Karbach⁹, J. Keaveney¹², I.R. Kenyon⁵⁵, U. Kerzel³⁷, T. Ketel²⁴, A. Keune³⁸, B. Khanji⁶, Y.M. Kim⁴⁶, M. Knecht³⁸, A. Kozlinskiy²³, L. Kravchuk³², K. Kreplin¹¹, M. Kreps⁴⁴, G. Krocker¹¹, P. Krokovny¹¹, F. Kruse⁹, K. Kruzelecki³⁷, M. Kucharczyk^{20,25,37,j}, T. Kvaratskheliya^{30,37}, V.N. La Thi³⁸, D. Lacarrere³⁷, G. Lafferty⁵⁰, A. Lai¹⁵, D. Lambert⁴⁶, R.W. Lambert²⁴, E. Lanciotti³⁷, G. Lanfranchi¹⁸, C. Langenbruch¹¹, T. Latham⁴⁴, C. Lazzeroni⁵⁵, R. Le Gac⁶, J. van Leerdam²³, J.-P. Lees⁴, R. Lefèvre⁵, A. Leflat^{31,37}, J. Lefrançois⁷, O. Leroy⁶, T. Lesiak²⁵, L. Li³, L. Li Gioi⁵, M. Lieng⁹, M. Liles⁴⁸, R. Lindner³⁷, C. Linn¹¹, B. Liu³, G. Liu³⁷, J. von Loeben²⁰, J.H. Lopes², E. Lopez Asamar³⁵, N. Lopez-March³⁸, H. Lu^{38,3}, J. Luisier³⁸, A. Mac Raighne⁴⁷, F. Machefert⁷, I.V. Machikhiliyan^{4,30}, F. Maciuc¹⁰, O. Maev^{29,37}, J. Magnin¹, S. Malde⁵¹, R.M.D. Mamunur³⁷, G. Manca^{15,d}, G. Mancinelli⁶, N. Mangiafave⁴³, U. Marconi¹⁴, R. Märki³⁸, J. Marks¹¹, G. Martellotti²², A. Martens⁸, L. Martin⁵¹, A. Martín Sánchez⁷, D. Martinez Santos³⁷, A. Massafferri¹, Z. Mathe¹², C. Matteuzzi²⁰, M. Matveev²⁹, E. Maurice⁶, B. Maynard⁵², A. Mazurov^{16,32,37}, G. McGregor⁵⁰, R. McNulty¹², M. Meissner¹¹, M. Merk²³, J. Merkel⁹, R. Messi^{21,k}, S. Miglieranzi³⁷, D.A. Milanese^{13,37}, M.-N. Minard⁴, J. Molina Rodriguez⁵⁴, S. Monteil⁵, D. Moran¹², P. Morawski²⁵, R. Mountain⁵², I. Mous²³, F. Muheim⁴⁶, K. Müller³⁹, R. Muresan^{28,38}, B. Muryn²⁶, B. Muster³⁸, M. Musy³⁵, J. Mylroie-Smith⁴⁸, P. Naik⁴², T. Nakada³⁸, R. Nandakumar⁴⁵, I. Nasteva¹, M. Nedos⁹, M. Needham⁴⁶, N. Neufeld³⁷, C. Nguyen-Mau^{38,o}, M. Nicol⁷, V. Niess⁵, N. Nikitin³¹, A. Nomerotski⁵¹, A. Novoselov³⁴, A. Oblakowska-Mucha²⁶, V. Obraztsov³⁴, S. Oggero²³, S. Ogilvy⁴⁷, O. Okhrimenko⁴¹, R. Oldeman^{15,d}, M. Orlandea²⁸, J.M. Otalora Goicochea², P. Owen⁴⁹, K. Pal⁵², J. Palacios³⁹, A. Palano^{13,b}, M. Palutan¹⁸, J. Panman³⁷, A. Papanestis⁴⁵, M. Pappagallo⁴⁷, C. Parkes^{50,37}, C.J. Parkinson⁴⁹, G. Passaleva¹⁷, G.D. Patel⁴⁸, M. Patel⁴⁹, S.K. Paterson⁴⁹, G.N. Patrick⁴⁵, C. Patrignani^{19,i}, C. Pavel-Nicorescu²⁸, A. Pazos Alvarez³⁶, A. Pellegrino²³, G. Penso^{22,l}, M. Pepe Altarelli³⁷, S. Perazzini^{14,c}, D.L. Perego^{20,j}, E. Perez Trigo³⁶, A. Pérez-Calero Yzquierdo³⁵, P. Perret⁵, M. Perrin-Terrin⁶, G. Pessina²⁰, A. Petrella^{16,37}, A. Petrolini^{19,i}, A. Phan⁵², E. Picatoste Olloqui³⁵, B. Pie Valls³⁵, B. Pietrzyk⁴, T. Pilař⁴⁴, D. Pinci²², R. Plackett⁴⁷, S. Playfer⁴⁶, M. Plo Casasus³⁶, G. Polok²⁵, A. Poluektov^{44,33}, E. Polycarpo², D. Popov¹⁰, B. Popovici²⁸, C. Potterat³⁵, A. Powell⁵¹, J. Prisciandaro³⁸, V. Pugatch⁴¹, A. Puig Navarro³⁵, W. Qian⁵², J.H. Rademacker⁴², B. Rakotomiaramanana³⁸, M.S. Rangel², I. Raniuk⁴⁰, G. Raven²⁴, S. Redford⁵¹, M.M. Reid⁴⁴, A.C. dos Reis¹, S. Ricciardi⁴⁵, K. Rinnert⁴⁸, D.A. Roa Romero⁵, P. Robbe⁷, E. Rodrigues^{47,50}, F. Rodrigues², P. Rodriguez Perez³⁶, G.J. Rogers⁴³, S. Roiser³⁷, V. Romanovsky³⁴, M. Rosello^{35,n}, J. Rouvinet³⁸, T. Ruf³⁷, H. Ruiz³⁵, G. Sabatino^{21,k}, J.J. Saborido Silva³⁶, N. Sagidova²⁹, P. Sail⁴⁷,

B. Saitta^{15,d}, C. Salzmann³⁹, M. Sannino^{19,i}, R. Santacesaria²², C. Santamarina Rios³⁶, R. Santinelli³⁷, E. Santovetti^{21,k}, M. Sapunov⁶, A. Sarti^{18,l}, C. Satriano^{22,m}, A. Satta²¹, M. Savrie^{16,e}, D. Savrina³⁰, P. Schaack⁴⁹, M. Schiller²⁴, S. Schleich⁹, M. Schlupp⁹, M. Schmelling¹⁰, B. Schmidt³⁷, O. Schneider^{38,*}, A. Schopper³⁷, M.-H. Schune⁷, R. Schwemmer³⁷, B. Sciascia¹⁸, A. Sciubba^{18,l}, M. Seco³⁶, A. Semennikov³⁰, K. Senderowska²⁶, I. Sepp⁴⁹, N. Serra³⁹, J. Serrano⁶, P. Seyfert¹¹, M. Shapkin³⁴, I. Shapoval^{40,37}, P. Shatalov³⁰, Y. Shcheglov²⁹, T. Shears⁴⁸, L. Shekhtman³³, O. Shevchenko⁴⁰, V. Shevchenko³⁰, A. Shires⁴⁹, R. Silva Coutinho⁴⁴, T. Skwarnicki⁵², A.C. Smith³⁷, N.A. Smith⁴⁸, E. Smith^{51,45}, K. Sobczak⁵, F.J.P. Soler⁴⁷, A. Solomin⁴², F. Soomro¹⁸, B. Souza De Paula², B. Spaan⁹, A. Sparkes⁴⁶, P. Spradlin⁴⁷, F. Stagni³⁷, S. Stahl¹¹, O. Steinkamp³⁹, S. Stoica²⁸, S. Stone^{52,37}, B. Storaci²³, M. Straticiuc²⁸, U. Straumann³⁹, V.K. Subbiah³⁷, S. Swientek⁹, M. Szczekowski²⁷, P. Szczypka³⁸, T. Szumlak²⁶, S. T'Jampens⁴, E. Teodorescu²⁸, F. Teubert³⁷, C. Thomas⁵¹, E. Thomas³⁷, J. van Tilburg¹¹, V. Tisserand⁴, M. Tobin³⁹, S. Topp-Joergensen⁵¹, N. Torr⁵¹, E. Tournefier^{4,49}, M.T. Tran³⁸, A. Tsaregorodtsev⁶, N. Tuning²³, M. Ubeda Garcia³⁷, A. Ukleja²⁷, P. Urquijo⁵², U. Uwer¹¹, V. Vagnoni¹⁴, G. Valenti¹⁴, R. Vazquez Gomez³⁵, P. Vazquez Regueiro³⁶, S. Vecchi¹⁶, J.J. Velthuis⁴², M. Veltri^{17,g}, B. Viaud⁷, I. Videau⁷, X. Vilasis-Cardona^{35,n}, J. Visniakov³⁶, A. Vollhardt³⁹, D. Volyanskyy¹⁰, D. Voong⁴², A. Vorobyev²⁹, H. Voss¹⁰, S. Wandernoth¹¹, J. Wang⁵², D.R. Ward⁴³, N.K. Watson⁵⁵, A.D. Webber⁵⁰, D. Websdale⁴⁹, M. Whitehead⁴⁴, D. Wiedner¹¹, L. Wiggers²³, G. Wilkinson⁵¹, M.P. Williams^{44,45}, M. Williams⁴⁹, F.F. Wilson⁴⁵, J. Wishahi⁹, M. Witek²⁵, W. Witzeling³⁷, S.A. Wotton⁴³, K. Wyllie³⁷, Y. Xie⁴⁶, F. Xing⁵¹, Z. Xing⁵², Z. Yang³, R. Young⁴⁶, O. Yushchenko³⁴, M. Zavertyaev^{10,a}, F. Zhang³, L. Zhang⁵², W.C. Zhang¹², Y. Zhang³, A. Zhelezov¹¹, L. Zhong³, E. Zverev³¹, A. Zvyagin³⁷

¹ Centro Brasileiro de Pesquisas Físicas (CBPF), Rio de Janeiro, Brazil

² Universidade Federal do Rio de Janeiro (UFRJ), Rio de Janeiro, Brazil

³ Center for High Energy Physics, Tsinghua University, Beijing, China

⁴ LAPP, Université de Savoie, CNRS/IN2P3, Annecy-Le-Vieux, France

⁵ Clermont Université, Université Blaise Pascal, CNRS/IN2P3, LPC, Clermont-Ferrand, France

⁶ CPPM, Aix-Marseille Université, CNRS/IN2P3, Marseille, France

⁷ LAL, Université Paris-Sud, CNRS/IN2P3, Orsay, France

⁸ LPNHE, Université Pierre et Marie Curie, Université Paris Diderot, CNRS/IN2P3, Paris, France

⁹ Fakultät Physik, Technische Universität Dortmund, Dortmund, Germany

¹⁰ Max-Planck-Institut für Kernphysik (MPIK), Heidelberg, Germany

¹¹ Physikalisches Institut, Ruprecht-Karls-Universität Heidelberg, Heidelberg, Germany

¹² School of Physics, University College Dublin, Dublin, Ireland

¹³ Sezione INFN di Bari, Bari, Italy

¹⁴ Sezione INFN di Bologna, Bologna, Italy

¹⁵ Sezione INFN di Cagliari, Cagliari, Italy

¹⁶ Sezione INFN di Ferrara, Ferrara, Italy

¹⁷ Sezione INFN di Firenze, Firenze, Italy

¹⁸ Laboratori Nazionali dell'INFN di Frascati, Frascati, Italy

¹⁹ Sezione INFN di Genova, Genova, Italy

²⁰ Sezione INFN di Milano Bicocca, Milano, Italy

²¹ Sezione INFN di Roma Tor Vergata, Roma, Italy

²² Sezione INFN di Roma La Sapienza, Roma, Italy

²³ Nikhef National Institute for Subatomic Physics, Amsterdam, The Netherlands

²⁴ Nikhef National Institute for Subatomic Physics and Vrije Universiteit, Amsterdam, The Netherlands

²⁵ Henryk Niewodniczanski Institute of Nuclear Physics Polish Academy of Sciences, Krakow, Poland

²⁶ AGH University of Science and Technology, Krakow, Poland

²⁷ Soltan Institute for Nuclear Studies, Warsaw, Poland

²⁸ Horia Hulubei National Institute of Physics and Nuclear Engineering, Bucharest-Magurele, Romania

²⁹ Petersburg Nuclear Physics Institute (PNPI), Gatchina, Russia

³⁰ Institute of Theoretical and Experimental Physics (ITEP), Moscow, Russia

³¹ Institute of Nuclear Physics, Moscow State University (SINP MSU), Moscow, Russia

³² Institute for Nuclear Research of the Russian Academy of Sciences (INR RAN), Moscow, Russia

³³ Budker Institute of Nuclear Physics (SB RAS) and Novosibirsk State University, Novosibirsk, Russia

³⁴ Institute for High Energy Physics (IHEP), Protvino, Russia

³⁵ Universitat de Barcelona, Barcelona, Spain

³⁶ Universidad de Santiago de Compostela, Santiago de Compostela, Spain

³⁷ European Organization for Nuclear Research (CERN), Geneva, Switzerland

³⁸ Ecole Polytechnique Fédérale de Lausanne (EPFL), Lausanne, Switzerland

³⁹ Physik-Institut, Universität Zürich, Zürich, Switzerland

⁴⁰ NSC Kharkiv Institute of Physics and Technology (NSC KIPT), Kharkiv, Ukraine

⁴¹ Institute for Nuclear Research of the National Academy of Sciences (KINR), Kyiv, Ukraine

⁴² H.H. Wills Physics Laboratory, University of Bristol, Bristol, United Kingdom

⁴³ Cavendish Laboratory, University of Cambridge, Cambridge, United Kingdom

⁴⁴ Department of Physics, University of Warwick, Coventry, United Kingdom

⁴⁵ STFC Rutherford Appleton Laboratory, Didcot, United Kingdom

⁴⁶ School of Physics and Astronomy, University of Edinburgh, Edinburgh, United Kingdom

⁴⁷ School of Physics and Astronomy, University of Glasgow, Glasgow, United Kingdom

⁴⁸ Oliver Lodge Laboratory, University of Liverpool, Liverpool, United Kingdom

⁴⁹ Imperial College London, London, United Kingdom

⁵⁰ School of Physics and Astronomy, University of Manchester, Manchester, United Kingdom

⁵¹ Department of Physics, University of Oxford, Oxford, United Kingdom

⁵² Syracuse University, Syracuse, NY, United States

⁵³ CC-IN2P3, CNRS/IN2P3, Lyon-Villeurbanne, France ^p

⁵⁴ Pontifícia Universidade Católica do Rio de Janeiro (PUC-Rio), Rio de Janeiro, Brazil ^q

⁵⁵ University of Birmingham, Birmingham, United Kingdom

⁵⁶ Physikalisches Institut, Universität Rostock, Rostock, Germany ^r

* Corresponding author.

E-mail address: Olivier.Schneider@epfl.ch (O. Schneider).

^a P.N. Lebedev Physical Institute, Russian Academy of Science (LPI RAS), Moscow, Russia.

^b Università di Bari, Bari, Italy.

^c Università di Bologna, Bologna, Italy.

^d Università di Cagliari, Cagliari, Italy.

^e Università di Ferrara, Ferrara, Italy.

^f Università di Firenze, Firenze, Italy.

^g Università di Urbino, Urbino, Italy.

^h Università di Modena e Reggio Emilia, Modena, Italy.

ⁱ Università di Genova, Genova, Italy.

^j Università di Milano Bicocca, Milano, Italy.

^k Università di Roma Tor Vergata, Roma, Italy.

^l Università di Roma La Sapienza, Roma, Italy.

^m Università della Basilicata, Potenza, Italy.

ⁿ LIFAELS, La Salle, Universitat Ramon Llull, Barcelona, Spain.

^o Hanoi University of Science, Hanoi, Viet Nam.

^p Associated member.

^q Associated to Universidade Federal do Rio de Janeiro (UFRJ), Rio de Janeiro, Brazil.

^r Associated to Physikalisches Institut, Ruprecht-Karls-Universität Heidelberg, Heidelberg, Germany.